Korean J. Chem. Eng., **21**(3), 712-720 (2004)

Effects of Adsorbate Properties on Adsorption Mechanism in a Carbon Molecular Sieve

Youn-Sang Bae, Jong-Ho Moon, Hyungwoong Ahn* and Chang-Ha Lee†

Dept. of Chem. Eng., Yonsei University, Seoul 120-749, Korea
*Department of Chemical Engineering, University College London, London, England
(*Received 9 February 2004 • accepted 2 April 2004*)

Abstract–The adsorption characteristics of six pure components (N_2, O_2, Ar, CO, H_2, and CH_4) on a CMS were studied over a wide pressure range up to 15 atm by using a volumetric method. Despite only relatively small differences in the kinetic diameters of the probe molecules used, very large differences in the magnitude of apparent time constants were observed. The adsorption kinetic characteristics of six components on the CMS were affected by the relative importance of atomic/molecular size, shape, and polar properties. Especially, the interaction properties of adsorbate molecules were proposed as an important factor to estimate the relative adsorption rate.

Key words: Carbon Molecular Sieve, Adsorption, Equilibria, Kinetics

INTRODUCTION

Recently, due to the increasing demand of high purity gases for fine chemical processing and electrical device processing, a strong economic motivation has prompted the development of adsorption processes to produce high purity products. Carbon molecular sieve (CMS) with pore sizes in the range of 3-5 Å is widely used for the production of high purity nitrogen from air by pressure swing adsorption (PSA) [Chen et al., 1994]. Different from most adsorbents in which the selectivity arises from the differences in adsorption equilibrium, the selectivity of CMS depends on the differences in adsorption kinetics [Ruthven, 1992].

When the size of an adsorbate molecule is close to the size of the micropore, the diffusion of the molecule becomes restricted and the diffusion in the micropore may have a significant effect on the overall adsorption rate. Thus, the diffusion in the micropore of CMS depends on adsorbate properties [Reid and Thomas, 1999; Kaneko, 1996].

Understanding the PSA process requires knowledge about both the equilibria and kinetics of adsorbates in an adsorbent [Yang and Lee, 1998; Ahn et al., 1999; Park, 2002; Choi et al., 2003; Kim et al., 2003; Panczyk and Rudzinski, 2004]. In addition, the deviation between PSA simulation and experimental data appeared to increase with increasing operating pressure in the air separation PSA with CMS because diffusivity had stronger dependence on surface coverage at wide pressure range [Gupta and Farooq, 1999]. However, most of the previous studies on CMS have focused on the low pressure range below 1 atm [Reid and Thomas, 1999; Rutherford and Do, 2000; O'koye et al., 1997; Chen and Yang, 1994; Do and Wang, 1998]. Since the PSA process is normally operated in the pressure range 1-15 atm, adsorption equilibria and kinetic data up to elevated pressures are needed to develop a well-designed adsorption process.

In this study, the adsorption equilibria and kinetics of the six components (N_2, O_2, Ar, CO, H_2, and CH_4) on the CMS, measured in the range of 293-313 K and 0-15 atm, were studied as a function of characteristics for each adsorbate. In addition, the interaction properties of molecules were investigated, and those were proposed as an important factor to estimate the relative sorption rate.

EXPERIMENTAL WORK

The adsorbent investigated in this study was a carbon molecular sieve (CMS-T3A) manufactured by Takeda Chemical Company. It was obtained in the form of extruded pellets of cylindrical shape. The average macropore size is about 0.27 μm and average micropore size is about 5 Å. The gases used as adsorbates were N_2, O_2, Ar, CO, H_2, and CH_4, and they were of high purity more than 99.9%.

The volumetric method was used to study the adsorption equi-

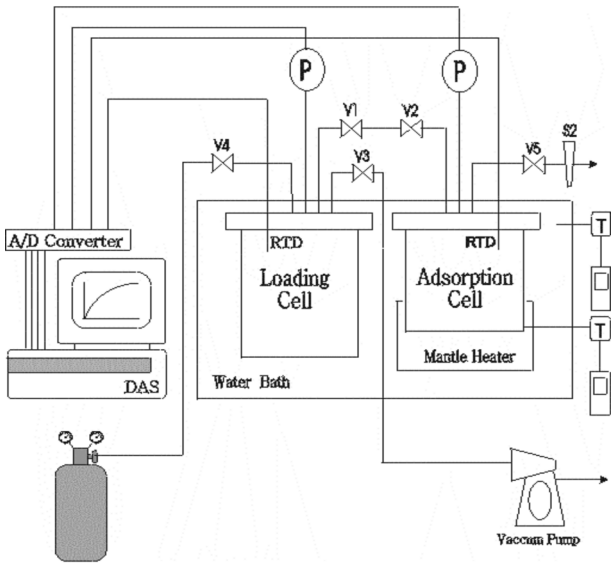

Fig. 1. Schematic diagram of experimental apparatus.
V: Ball valve
S: Sampling port
P: Pressure transducer
T: Thermocouple and temperature controller
DAS: Data aquisition system
RTD: Residence temperature detector

†To whom correspondence should be addressed.
E-mail: leech@yonsei.ac.kr

libria and the sorption kinetics. A schematic diagram of the apparatus is shown in Fig. 1. The adsorption isotherms and the apparent time constants were measured by the stepwise pressure change. Prior to each experiment, the adsorbent was regenerated by evacuation at 423.5 K during 12 hrs. The instrument and experimental procedure have been described in detail previously [Bae et al., 2003].

The adsorbed amounts per unit adsorbent weight (n) were calculated by the following mass balance for a pure gas:

$$\left.\frac{P_d V_d}{Z_d R T_d}\right|_1 + \left.\frac{P_a V_a}{Z_a R T_a}\right|_1 = \left.\frac{P_d V_d}{Z_d R T_d}\right|_2 + \left.\frac{P_a V_a}{Z_a R T_a}\right|_2 + Mn \tag{1}$$

where P is the gas pressure (atm), T is the temperature (K), V is the volume (L), Z is the compressibility factor (-), R is the gas constant (0.082 L atm mol^{-1} K^{-1}) and M is the weight of the adsorbent. The subscripts 1, 2, d and a indicate the initial state, the final state, the dosing cell and the adsorption cell, respectively. The compressibility factor, Z, is obtained as follows [Smith et al., 1997]:

$$Z = 1 + \left(0.083 - \frac{0.422}{T_r^{1.6}}\right)\frac{P_r}{T_r} + \omega\left(0.139 - \frac{0.172}{T_r^{4.2}}\right)\frac{P_r}{T_r} \tag{2}$$

where P_r is the reduced pressure, T_r is the reduced temperature, and ω is the acentric factor.

MATHEMATICAL MODELS

1. Equilibrium Model

The isotherms of all the gases except H_2 show considerable curvature in the pressure range of the PSA process. These type I isotherms can be fitted to a good approximation by the Toth model.

The Toth isotherm is a semi-empirical expression that effectively describes many systems with submonolayer coverage, Because of its simplicity in form and its correct behavior at low and high pressures, the Toth equation is recommended as the first choice of an isotherm equation for fitting the data of many adsorbates on carbon molecular sieve as well as activated carbon and zeolite [Do, 1988]. It is a three parameter model usually written in the following form:

$$q = \frac{q_m P}{(b + P^t)^{1/t}} \tag{3}$$

Where P is the equilibrium pressure, q is the number of adsorbed moles, and q_m, b, and t are isotherm parameters that are determined numerically. When the parameter t is unity, the above equation is identical with the Langmuir equation. Also, the Toth equation reduces to the Henry's law at low pressures and approaches the saturation limit at high pressures.

2. Kinetic Model

In the experiments of the constant-volume-variable-pressure method [Bülow and Micke, 1994, 1995; Micke et al., 1994], batch adsorption takes place in a vessel with finite volume. Hence, concentration of an adsorbate in the vessel decreases with progress of adsorption. Basic equations to describe sorption uptake phenomena in vessels consist of a set of mass balance equations.

Bülow and Micke [1994] proposed a non-linear Volterra integral technique, and by this method, it was possible to obtain correct sorption kinetic parameters by constant-volume-variable-pressure method. However, this method has the need to describe the flow through the valve accurately.

Recently, Brandani [Brandani, 1998] proposed an excellent model for the directive calculation of apparent time constants from the pressure data of dosing and adsorption cells. This method eliminates the need to describe the flow through the valve.

The experimental method in this model follows the transient pressure response when a sample of adsorbent is subjected to a change in adsorbate pressure.

The assumptions for this model are as follows:

(1) The adsorbent has micropores and both crystals and pellets are spherical.
(2) The gases follow the ideal gas behavior.
(3) The system is in an isothermal condition.
(4) The valve between two cells is considered ideal (opening time =0).
(5) The apparent time constants are considered uniform during an uptake.

Under these assumptions, the mass balance of the adsorption cell is given by

$$V_s \frac{\partial \bar{q}}{\partial t} + \epsilon V_a \frac{\partial c}{\partial t} = \frac{\partial n}{\partial t} \tag{4}$$

The first term in the left side is the change of moles in the adsorbent, the second term is the change of moles in the adsorption cell, and the term in the right side is the moles change in the dosing cell.

Considering an ideal gas behavior, the following relation can be applied for the dosing cell.

$$\frac{\partial n}{\partial t} = -\frac{V_d}{R T_d}\frac{\partial P_d}{\partial t} \tag{5}$$

The mass balance in the adsorbent particles, considering spherical form, is given by

$$\frac{\partial \bar{q}}{\partial t} = \frac{3D}{R}\left(\frac{\partial q}{\partial r}\right)_{r=R} \qquad \frac{\partial q}{\partial t} = D\left(\frac{\partial^2 q}{\partial r^2} + \frac{2}{r}\frac{\partial q}{\partial r}\right) \tag{6}$$

The following conditions are considered as boundary conditions on Eq. (6):

The surface between the adsorbed phase and the gas phase is in equilibrium. (7a)

$$\left(\frac{\partial q}{\partial r}\right)_{r=0} = 0 \tag{7b}$$

In order to obtain an analytical solution, the following linear equilibrium relationship is assumed:

$$q(R, t) - q_0 = H(c(t) - c_0) \tag{8}$$

where H is equilibrium constant. The left side of the above equation represents the concentration change of adsorbed phase and the right side represents the concentration change of gas phase. In this study, each step in the uptake experiment is regarded as being in the linear range.

To represent the exact solution by a dimensionless form, the following dimensionless variables are defined as follows.

$$\tau=\frac{tD}{R^2};\qquad Q=\frac{q-q_0}{q_\infty-q_0};\qquad \rho_d=\frac{P_d-P_a^0}{P_\infty-P_a^0};$$
$$\rho_u=\frac{P_a-P_a^0}{P_\infty-P_a^0};\qquad \gamma=\frac{1\in V_a}{3HV_s};\qquad \delta=\frac{1}{3H}\frac{V_d}{V_s};\qquad (9)$$

Where τ is the dimensionless time, Q is the dimensionless adsorbed phase concentration, ρ_d is the reduced pressure of dosing cell and ρ_a is the reduced pressure of adsorption cell. The notation γ represents the ratio of the adsorbate accumulation in the adsorption cell to that in the adsorbent. Also, δ represents the ratio of the adsorbate accumulation in the dosing cell to that in the adsorbent.

It is possible to analyze the pressure uptake curves without the need for an accurate description of the flow through the valve only if the pressures in both dosing and adsorption cells are monitored [Brandani, 1998]. This can be accomplished by using the following overall mass balance considering a concentration independent diffusivity:

$$\frac{\rho_d}{\rho_d^0}=1-\frac{\gamma\rho_a}{\delta\rho_d^0}-\sum_{n=1}^{\infty}\int_0^{\tau}\exp[n^2\pi^2(u-\tau)]\frac{\rho_a(u)}{\rho_d^0}du \qquad (10)$$

This equation allows one to predict the pressure in the dosing cell from the experimental pressure in the adsorption cell. If the pressure in the adsorption cell exhibits a distinct maximum, it is possible to obtain the apparent time constant, which is the only unknown parameter. Since the information of the flow through the valve is the experimentally obtained pressure in the adsorption cell, the predicted pressure in the dosing cell will only depend on the intracrystalline mass transfer.

RESULTS AND DISCUSSION

1. Adsorption Equilibria

The adsorption isotherms of six different gas molecules at 303 K were compared in Fig. 2. As shown in Fig. 2, CH_4 showed the largest adsorption capacity and the most favorable isotherm on the CMS. Also, CO, Ar, O_2 and N_2 showed similar adsorption capacities and isotherm shapes with each other. However, CO showed a slightly more favorable isotherm on the CMS. Therefore, it seems that these gases might be hard to separate by the difference in adsorption equilibrium on CMS. In the case of H_2, it showed the linear isotherm, and the adsorption capacity of H_2 on the CMS was the smallest. All the equilibrium data were well predicted by Toth isotherm. The data of adsorption equilibrium obtained from this study are almost similar with those of the previous papers measured in the low pressure range [Chen et al., 1994; Ruthven, 1992; Srinivasan et al., 1995; Ruthven et al., 1986; Rynders et al., 1997; O'koye et al., 1997].

To explain the adsorption kinetic phenomena on the CMS at the later section, it is meaningful to investigate the adsorption interactions between adsorbent and adsorbate and between the adsorbed molecules. In this study, isosteric heat of adsorption and virial equation were applied to the adsorption interactions.

Previous studies proposed that the relation between isosteric heat and coverage somewhat explains the interaction properties in the heterogeneous surface [Ross and Oliver, 1964; Talu and Kabel, 1987]. According to the ideal Langmuir model, the heats of adsorption are independent of the change of the coverage. In real adsorption systems, however, they are dependent on the coverage. This is owing to the heterogeneity of surface energy and the lateral interactions between adsorbates [Ross and Oliver, 1964]. For heterogeneous surfaces in the micropores of some adsorbents such as CMS and activated carbon, vertical interactions between the solid surface molecules and gas molecules decrease as coverage increases, while lateral interactions between the adsorbed molecules increase with coverage [Chen et al., 1994]. These give the useful information about the characteristics of the adsorbed surface and the adsorbed phase.

In this study, the isosteric heat of adsorption ($-\Delta H_s$) was calculated from the temperature dependence of the equilibrium capacity using the following Clausius-Clapeyron equation from the Toth isotherm [Suzuki, 1990].

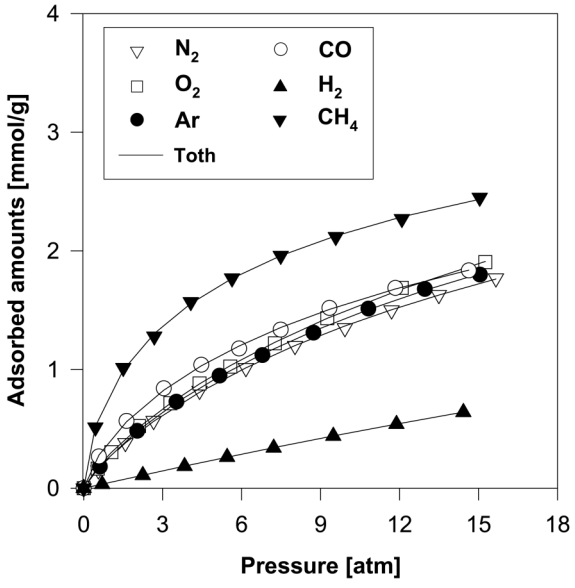

Fig. 2. Adsorption isotherms of six pure gases (N_2, O_2, Ar, CO, H_2, and CH_4) at 303 K and the fits of the Toth isotherm.

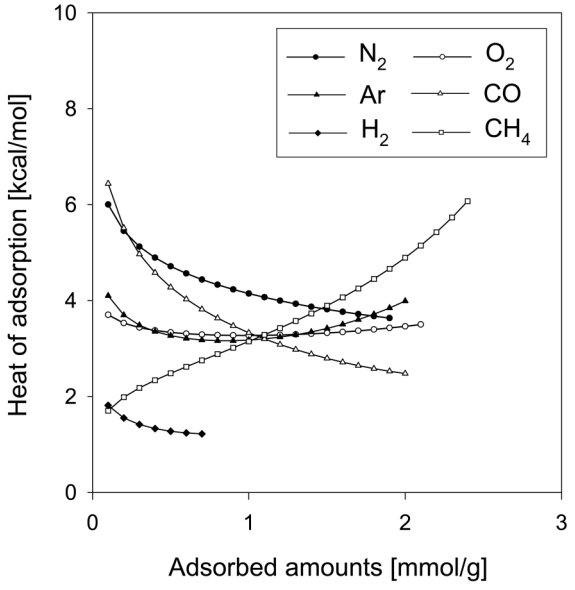

Fig. 3. Isosteric heats of adsorption for six gases (N_2, O_2, Ar, CO, H_2, and CH_4).

$$\left(\frac{d\ln P}{dT}\right)_n = \frac{-\Delta H_s}{RT^2} \quad (11)$$

In Fig. 3, the heats of adsorption of six adsorbates are shown as the functions of the adsorbed amounts. CO shows a steep decrease in $-\Delta H_s$ as coverage increases. In the cases of N_2 and H_2, $-\Delta H_s$ is slightly decreased as coverage increases. This implies that the vertical interaction is a dominating factor in adsorption of these components, especially CO. On the other hand, CH_4 shows a steep increase in $-\Delta H_s$ with an increase in the coverage. It may be noted that the lateral interaction in the CH_4 adsorption is dominant. In the cases of Ar and O_2, the heat of adsorption slightly decreases at low coverage range while it slightly increases at high coverage range. Therefore, it seems that the adsorption phenomena in these components change from vertical interaction to lateral interaction with an increase in the coverage.

On the other hand, in this study, the interactions in the micropore were also explained by the virial equation. The equilibrium result for each gas was fitted by virial equation as follows [Reid and Thomas, 1999]:

$$\ln(n/p) = A_0 + A_1 n \quad (12)$$

where n is the adsorbed amounts per unit adsorbent mass (mol/g), and p is the gas pressure (Pa). The first virial coefficient, A_0, is related to the Henry's law constant, K_0, by the equation, $K_0 = \exp(A_0)$. Since the K_0 depends on the extent of adsorption, it depends on the interaction between the adsorbent surface and the adsorbed molecule. Also, the second virial coefficient, A_1, is related to the interaction between the pairs of molecules under the influence of surface forces. In this study, the higher terms (A_2, etc.) in the virial equation were ignored.

All the virial coefficients for each gas are presented in Table 1. Fig. 4 shows the virial results for Ar at 293 K, 303 K, and 313 K as one of the examples. This figure shows more or less linear tendency in the virial graphs over the experimental pressure range, but shows some deviations at low-pressure where Henry's law is obeyed. Reid et al. [1998] reported that the virial parameters for Ar at 0-9 atm on the CMS from Air Products and Chemicals Co. were −19.902 for A_0 (mol g^{-1} Pa^{-1}) at 313 K and −696 for A_1 (g mol^{-1}) at 313 K. These values were similar to the results of this study as shown in Table 1. Also, compared with the results of the literature, the values of A_0 and A_1 for O_2, N_2, and CO were similar with those presented in Table 1, even though the results in this study were obtained from

Table 1. Virial parameters for adsorption of six gases on CMS

	A_0/(mol g^{-1} Pa^{-1})					
Temp.	N_2	O_2	Ar	CO	H_2	CH_4
293 K	−19.276	−19.420	−19.424	−18.757	−21.309	−18.060
303 K	−19.665	−19.555	−19.606	−19.029	−21.442	−17.815
313 K	−19.788	−19.751	−19.730	−19.266	−21.543	−18.161
	A_1/[g mol^{-1}] (Pa^{-1})					
Temp.	N_2	O_2	Ar	CO	H_2	CH_4
293 K	−647.5	−476.0	−515.0	−875.7	−258.7	−750.4
303 K	−548.2	−519.6	−535.3	−818.9	−122.6	−1,004.3
313 K	−544.0	−501.5	−570.2	−750.8	−73.5	−964.3

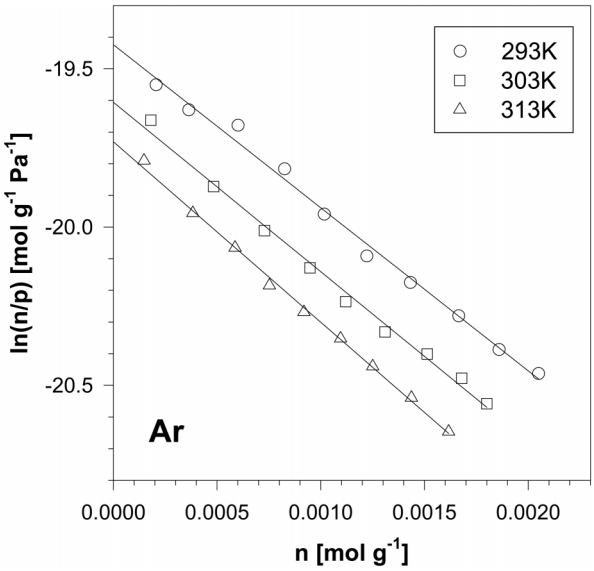

Fig. 4. Virial graphs for the adsorptions of Ar at 293 K, 303 K, and 313 K.

the high pressure range, 0-15 atm. Therefore, it seems that virial graphs in the low-pressure range might be extended to the high-pressure range. However, since the virial graphs in Fig. 4 slightly deviate from linearity at round 0.5 atm, it might be hard to extend the virial graphs to the ultra-low pressure range.

As shown in Table 1, the order of the first virial coefficient (A_0) for the six adsorbates was as follows: CH_4>CO>N_2, O_2, Ar>H_2. Also, the order of the second virial coefficient (A_1) was as follows: CH_4<CO<N_2<Ar<O_2<H_2. The order of A_0 coincided with the order of the adsorbed amount of each adsorbate. Also, the virial parameters obtained from N_2, O_2, and Ar were within a similar range. The values of A_0 for CO and CH_4 were higher than those for the other adsorbates due to much the higher adsorption amount at low pressure.

2. Adsorption Kinetics

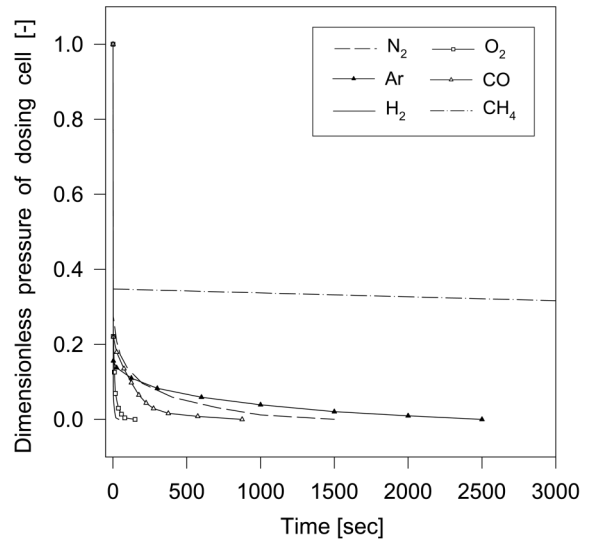

Fig. 5. Dimensionless pressure histories of dosing cell for six gases (N_2, O_2, Ar, CO, H_2, and CH_4) at 303 K, 0.2-0.7 atm.

Fig. 5 shows the experimental dimensionless pressure histories of the dosing cell at 303 K for (a) N_2 (0-0.52 atm), (b) O_2 (0-0.51 atm), (c) Ar (0-0.61 atm), (d) CO (0-0.67 atm,), (e) H_2 (0-0.70 atm), (f) CH_4 (0-0.50 atm). As shown in this figure, each adsorbate showed a different pressure history on the CMS. Also, the time taken for each gas to reach adsorption equilibrium was different. Especially, it took a long time (about 40 hr) for CH_4 to approach the adsorption equilibrium.

The apparent time constants, D/r^2, were calculated from Eq. (10) with the transient pressure of dosing and adsorption cells. The values of D/r^2 were obtained from nonlinear regression by using the least-square method.

To confirm the validity of the experimental results measured by the volumetric method in this study, the results of N_2 and O_2 are compared with the published data obtained from a gravimetric method in Fig. 6 [Reid and Thomas, 1999; Reid et al., 1998]. Considering the difference in manufacturing companies for CMS, both results are reasonably similar at low-pressure range. Also, Fig. 6 shows that the adsorption rates of N_2 and O_2 began to increase steeply in the range of 10 and 7 atm, respectively. Furthermore, comparing the pressure dependence of the adsorption rate, it shows a relatively weak temperature dependence on the CMS used in this study. On the other hand, the rate data of N_2 and O_2 for the CMS have been reported previously in many published papers measured at the low pressure range. The results are compared with the results of the present study in Table 2. The apparent time constants measured by var-

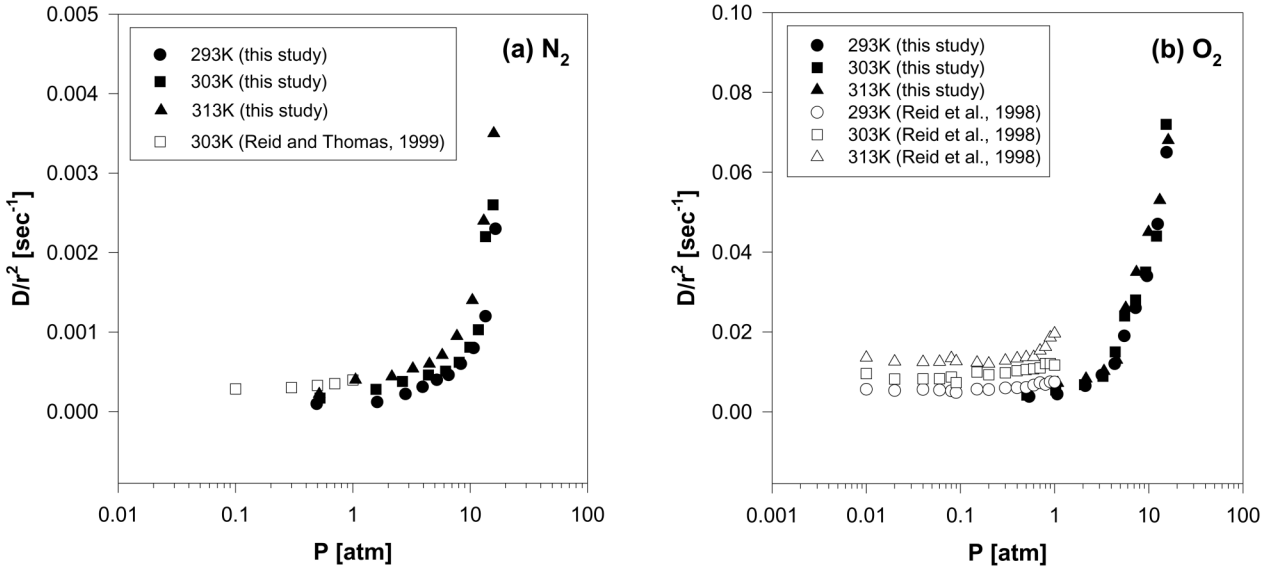

Fig. 6. Comparisons of the apparent time constants from this study and those from the study of Reid and Thomas [1999] and Reid et al. [1998] for the cases of (a) N_2, and (b) O_2.

Table 2. Apparent time constants for O_2 and N_2 adsorptions on CMS in the previous literature and this work

Author [year]	Method (Adsorbent)	Sorbate	Temp.	Diffusivity	Kinetic selectivity
Ruthven et al. [1986]	Gravimetric (B-F)	O_2	303 K	$D/r^2=3.7\times10^{-3}$ sec^{-1}	30.8
		N_2	303 K	$D/r^2=1.2\times10^{-4}$ sec^{-1}	
			273 K	$D/r^2=4.5\times10^{-5}$ sec^{-1}	
Ruthven [1992]	Gravimetric (B-F)	O_2	273 K	$D/r^2=2.4\times10^{-4}$ sec^{-1}	68.6
		N_2	273 K	$D/r^2=3.5\times10^{-6}$ sec^{-1}	
Chen et al. [1994]	DAB (B-F)	O_2	300 K	$D/r^2=3.5\times10^{-4}$ sec^{-1}	36.8
		N_2	300 K	$D/r^2=9.5\times10^{-6}$ sec^{-1}	
Srinivasan et al. [1995]	Volumetric (B-F)	O_2	293 K		30-40
		N_2	293 K		
Rynders et al. [1997]	IET (Takeda)	O_2	303 K	$k=6.0\times10^{-2}$ sec^{-1}	21.9
		N_2	303 K	$k=3.2\times10^{-3}$ sec^{-1}	
O'koye et al. [1997]	Gravimetric (APCI)	O_2	293 K	$k=1.05\times10^{-2}$ sec^{-1}	37.5
		N_2	293 K	$k=2.8\times10^{-4}$ sec^{-1}	
Yuxun and Farooq [1998]	Finite volume method (Takeda)	O_2	302-323 K	$D/r^2=7.45\times10^{-3}$ sec^{-1}	31.7
		N_2	302-323 K	$D/r^2=2.35\times10^{-4}$ sec^{-1}	
This work	Volumetric (Takeda)	O_2	293 K	$D/r^2=3.8\times10^{-3}$ sec^{-1}	38.0
		N_2	293 K	$D/r^2=1.0\times10^{-4}$ sec^{-1}	

Table 3. Apparent time constants (D/r^2) for N_2 adsorption on CMS

293 K		303 K		313 K	
Pressure [atm]	D/r^2 [10^{-4} sec^{-1}]	Pressure [atm]	D/r^2 [10^{-4} sec^{-1}]	Pressure [atm]	D/r^2 [10^{-4} sec^{-1}]
0.00-0.49	1.0	0.00-0.52	1.7	0.00-0.52	2.2
0.49-1.61	1.2	0.52-1.57	2.8	0.52-1.05	4.0
1.61-2.81	2.2	1.57-2.65	3.8	1.05-2.15	4.4
2.81-3.94	3.1	2.65-4.41	4.6	2.15-3.25	5.4
3.94-5.20	4.0	4.41-6.18	5.1	3.25-4.49	6.0
5.20-6.55	4.6	6.18-8.05	6.2	4.49-5.79	7.1
6.55-8.34	6.2	8.05-9.94	8.1	5.79-7.70	9.5
8.34-10.71	8.1	9.94-11.74	10.3	7.70-10.44	14.3
10.71-13.50	11.8	11.74-13.52	21.9	10.44-13.06	23.7
13.50-16.43	23.2	13.52-15.69	26.0	13.06-15.91	35.1

Table 4. Apparent time constants (D/r^2) for O_2 adsorption on CMS

293 K		303 K		313 K	
Pressure [atm]	D/r^2 [10^{-4} sec^{-1}]	Pressure [atm]	D/r^2 [10^{-4} sec^{-1}]	Pressure [atm]	D/r^2 [10^{-4} sec^{-1}]
0.00-0.54	38.3	0.00-0.51	42.1	0.00-0.53	45.8
0.54-1.07	44.0	0.51-1.03	54.4	0.53-1.08	72.1
1.07-2.12	64.8	1.03-2.08	67.9	1.08-2.16	82.9
2.12-3.18	92.1	2.08-3.27	89.0	2.16-3.35	102
3.18-4.35	122	3.27-4.41	151	3.35-4.57	130
4.35-5.50	189	4.41-5.57	240	4.57-5.70	259
5.50-7.28	261	5.57-7.26	279	5.70-7.40	353
7.28-9.60	338	7.26-9.27	353	7.40-9.96	447
9.60-12.46	467	9.27-12.13	437	9.96-13.11	530
12.46-15.49	652	12.13-15.32	722	13.11-16.14	683

Table 5. Apparent time constants (D/r^2) for Ar adsorption on CMS

293 K		303 K		313 K	
Pressure [atm]	D/r^2 [10^{-4} sec^{-1}]	Pressure [atm]	D/r^2 [10^{-4} sec^{-1}]	Pressure [atm]	D/r^2 [10^{-4} sec^{-1}]
0.00-0.62	0.9	0.00-0.61	0.7	0.00-0.58	0.9
0.62-1.18	1.0	0.61-2.03	1.7	0.58-1.77	1.9
1.18-2.08	1.5	2.03-3.52	2.3	1.77-3.00	2.3
2.08-3.31	2.1	3.52-5.15	2.9	3.00-4.34	3.3
3.31-4.68	2.8	5.15-6.77	4.2	4.34-5.76	3.9
4.68-6.42	3.4	6.77-8.71	5.9	5.76-7.46	4.6
6.42-8.19	4.2	8.71-10.77	6.8	7.46-9.28	5.7
8.19-10.56	5.8	10.77-12.89	8.1	9.28-11.79	8.2
10.56-13.12	7.8	12.89-15.00	11.3	11.79-14.76	142
13.12-15.60	12.1				

ious methods are much different from each other as shown in Table 2. However, the ratios of the apparent time constants of N_2 and O_2 are similar to that obtained from the present results and this proves the validity of this study. Also, the order in the adsorption rates based on pressure change were similar with the results in the literature for the adsorption rates of O_2, CO, N_2, Ar, and CH_4 on various CMS such as AP-CMS, BF-CMS, and CMS-T3A [Reid and Thomas, 1999; Rutherford and Do, 2000; Ruthven, 1992; Reid et al., 1998; Chen et al., 1994; Kapoor and Yang, 1989].

Apparent time constants of N_2, O_2, Ar, CO, and CH_4 at 0-15 atm and 293-313 K are shown in Tables 3 to 7, respectively. In the case of H_2, the sorption rates were too fast to obtain these values. Despite only relatively small changes in the size of the molecules used, very large changes in the magnitude of the apparent time constants were observed. Also, the apparent time constants of all the adsorbates on the CMS showed strong pressure dependence. Moreover, the adsorption rates were steeply increased at the different pressure range depending on the adsorbate.

In Fig. 7, the apparent time constants of O_2, N_2, and Ar at 293 K are compared. The adsorption rate of O_2 is about 30-40 times faster

Table 6. Apparent time constants (D/r^2) for CO adsorption on CMS

293 K		303 K		313 K	
Pressure [atm]	D/r^2 [10^{-4} sec^{-1}]	Pressure [atm]	D/r^2 [10^{-4} sec^{-1}]	Pressure [atm]	D/r^2 [10^{-4} sec^{-1}]
0.00-0.56	2.5	0.00-0.60	3.2	0.00-0.67	3.6
0.56-1.64	3.6	0.60-1.64	4.0	0.67-2.05	5.5
1.64-3.02	5.5	1.64-3.06	7.3	2.05-3.57	8.5
3.02-4.43	7.4	3.06-4.48	10.1	3.57-5.13	11.2
4.43-6.00	10.2	4.48-5.91	15.0	5.13-6.65	16.8
6.00-7.78	18.3	5.91-7.50	29.8	6.65-8.70	23.2
7.78-10.14	37.1	7.50-9.37	43.5	8.70-10.87	41.8
10.14-12.42	66.8	9.37-11.85	63.0	10.87-13.00	59.1
12.42-14.94	78.2	11.85-14.65	72.8	13.00-15.35	84.0

Table 7. Apparent time constants (D/r^2) for CH_4 adsorption on CMS

293 K		303 K		313 K	
Pressure [atm]	D/r^2 [10^{-4} sec^{-1}]	Pressure [atm]	D/r^2 [10^{-4} sec^{-1}]	Pressure [atm]	D/r^2 [10^{-4} sec^{-1}]
0.00-0.52	0.0032	0.00-0.47	0.0041	0.00-0.50	0.0053
0.52-1.69	0.0066	0.47-1.53	0.0124	0.50-1.83	0.0132
1.69-3.04	0.0354	1.53-2.69	0.0303	1.83-3.21	0.0273
3.04-4.49	0.0717	2.69-4.05	0.0552	3.21-4.76	0.0708
4.49-6.05	0.110	4.05-5.65	0.0889	4.76-6.33	0.151
6.05-7.94	0.162	5.65-7.47	0.133	6.33-8.21	0.252
7.94-10.28	0.254	7.47-9.61	0.247	8.21-10.70	0.399
10.28-12.60	0.369	9.61-12.09	0.381	10.70-13.30	0.554
12.60-15.23	0.543	12.09-15.03	0.532	13.30-15.73	0.631

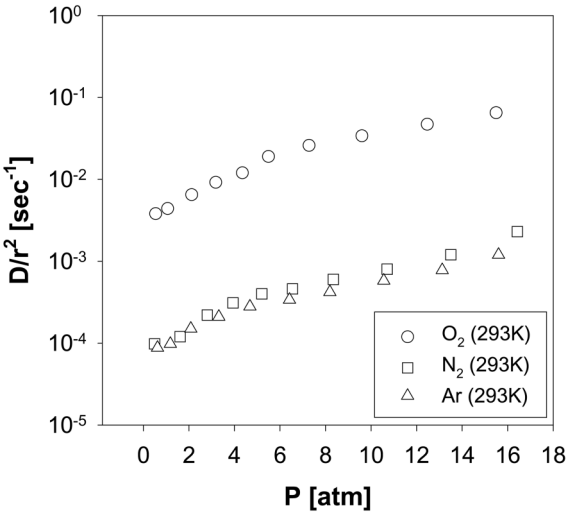

Fig. 7. Apparent time constants of O_2, N_2 and Ar at 293 K.

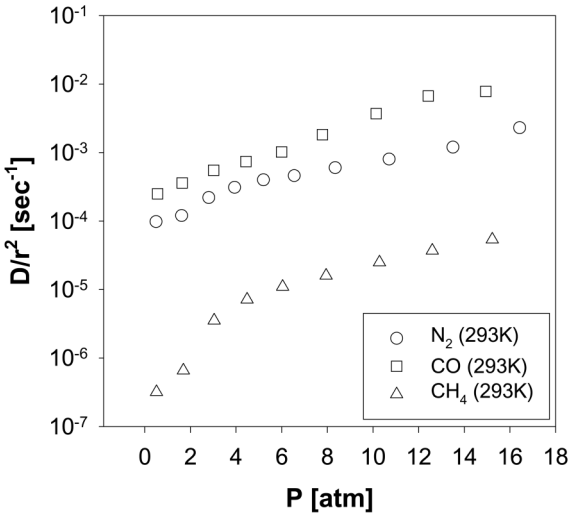

Fig. 8. Apparent time constants of N_2, CO, and Ar at 293 K.

than that of N_2 and Ar. Using the fast adsorption of O_2 compared with that of N_2, this CMS can be effectively used for N_2 separation from air by PSA process. However, owing to the similar adsorption rates of N_2 and Ar, an additional zeolite bed for removing Ar from N_2 is needed to obtain N_2 with high purity.

On the other hand, the apparent time constants of N_2, CO and CH_4 at 293 K are compared in Fig. 8. The adsorption rate of CH_4 is about 40-80 times slower than that of N_2 and CO. Using the slow adsorption of CH_4 compared with those of N_2 and CO, this CMS can be effectively used for CH_4 separation from coke oven gas (COG) by PSA process.

At the same temperature (293 K) and the similar pressure (around 0.5 atm), the order of the apparent time constants of five adsorbates was as follows: O_2 (38.3)>CO (2.5)>N_2 (1.0)>Ar (0.9)>CH_4 (0.0032) based on the 10^{-4} sec^{-1} unit.

In the low pressure range, the adsorption rate of CH_4 was remark-

ably slow, even though the kinetic diameter of CH_4 (3.82 Å) is not much larger than that of N_2 (3.68 Å). Also, the adsorption rate of Ar was about 40 times slower than that of O_2, even though the kinetic diameters of both adsorbates are similar (Ar : 3.42 Å, O_2 : 3.43 Å). Therefore, the kinetics of Ar and CH_4 could not be simply explained by the kinetic diameter.

It has been reported in the literature [Reid and Thomas, 1999; Kaneko, 1996] that the difference in the adsorption kinetics is mainly related to molecular size, shape, and electronic structure.

In this study, CH_4 and Ar have tetrahedral and spherical structures, respectively, and the other molecules have linear structure. The slow adsorption rates of CH_4 and Ar can be explained by their non-linear molecular structures.

On the other hand, CO has a dipole moment (0.117D) and a quadrupole moment (8.3 cm^2), N_2 has a quadrupole moment (4.7 cm^2), and O_2 has spin-spin interactions between molecules [Reid and Thomas, 1999; Rutherford and Do, 2000]. However, both CH_4 and Ar have no electronic properties. Therefore, the slow adsorption rates of CH_4 and Ar also can be explained by their stable electronic structures.

In addition, as we reported in the previous section, lateral interaction is dominant in the CH_4 adsorption. The lateral interactions between CH_4 molecules seem to interrupt the adsorption of adsorbate molecules on the surface of adsorbent, and to induce the extremely slow adsorption of CH_4. On the contrary, vertical interaction is dominant in the adsorptions of N_2, CO, and H_2. The relatively faster sorptions of N_2 and CO than that of Ar can be explained by their vertical interactions.

From these results, all the factors related to the adsorption rates can be summarized as in Table 8. The adsorption rates get faster as vertical interaction, dipole or quadrupole moments are larger, respectively. On the other hand, the adsorption rates get slower as kinetic diameter and lateral interaction are larger, respectively. Furthermore, the non-linear molecular structure strongly affects the adsorption rate to become much slower than the linear structure.

CONCLUSIONS

Adsorption equilibrium and kinetics of six components on carbon molecular sieve were obtained at the wide ranges of temperature and pressure by the volumetric method.

From the change of isosteric heat of adsorption ($-\Delta H_s$) with surface coverage, the dominant interaction of each gas was estimated. A strong vertical interaction was dominant for CO adsorption while a lateral interaction was dominant for CH_4 adsorption.

Despite only relatively small changes in the size of the probe molecules, very large changes in the magnitude of the adsorption rate were observed. Also, the difference in the kinetic diameter was not enough to explain the kinetic separation because the order of adsorption rate did not coincide with the kinetic diameter sequence. The adsorption kinetic characteristics on the CMS were affected by the relative importance of various factors. The adsorption rate of the linear molecules was faster than that of the non-linear ones. Also, the polar properties of adsorbate molecules seem to induce a high sorption rate. Especially, the interaction properties of adsorbate molecules were proposed as an important factor to estimate the relative adsorption rate. The adsorption rates seem to get faster as the effect of vertical interaction is larger. On the contrary, the adsorption rates seem to get slower as the effect of lateral interaction is larger.

ACKNOWLEDGMENTS

The financial support of the Carbon Dioxide Reduction and Sequestration R & D Center (C002-0103-001-1-0-0) is gratefully acknowledged.

NOMENCLATURE

b : equilibrium parameter for Toth model [atm^{-1}]
c : gas-phase concentration in bulk phase [mol/cm^3]
D : diffusivity [cm^2/sec]
H : equilibrium constant
n : moles in dosing cell [mol]; amount adsorbed in moles [mmol/g]
P : gas pressure [atm]
q, q_s, $\bar{q}$: amount adsorbed, equilibrium amount adsorbed [mmol/g], and average adsorbed phase concentration [mol/m^3], respectively
r : radial distance in pellet [cm]
R : radius of crystals [cm]
V : volume [cm^3]

Greek Letter

ε : void fraction in uptake cell

Superscript

0 : initial value

Subscripts

a : adsorption cell
d : dosing cell

Table 8. The factors influencing on adsorption rate

Properties	Factors	Adsorption rate
Size of adsorbate	Kinetic diameter	− dependence
Dominating interactions	Vertical interaction	+ dependence
	Lateral interaction	− dependence
Polar properties of adsorbate	Dipole or quadrupole moments	+ dependence
	Polarizability	+ dependence
Shape of adsorbate	Structure	Sphere→slow
		Linear→fast

s : solid
∞ : final value at equilibrium

REFERENCES

Ahn, H., Lee, C. H., Seo, B. K., Yang, J. Y. and Baek, K. H., "Backfill Cycle of a Layered Bed H_2 PSA Process," *Adsorption*, **5**, 419 (1999).

Bae, Y. S., Ryu, Y. and Lee, C. H., "Pressure-Dependent Models for Adsorption Kinetics on a CMS," Adsorption Science and Technology, Lee, C. H., eds., World Scientific, Singapore, 167 (2003).

Brandani, S., "Analysis of the Piezometric Method for the Study of Diffusion in Microporous Solids: Isothermal Case," *Adsorption*, **4**, 17 (1998).

Bülow, M. and Micke, A., "Determination of Transport Coefficients in Microporous Solids," *Adsorption*, **1**, 29 (1995).

Bülow, M. and Micke, A., "Intracrystalline Diffusion of Benzene in Microporous Gallosilicate with MFI Structure," *J.C.S. Faraday Trans*., **90**, 2585 (1994).

Chen, Y. D., Yang, R. T. and Uawithya, P., "Diffusion of Oxygen, Nitrogen and Their Mixtures in Carbon Molecular Sieve," *AIChE J*., **40**, 577 (1994).

Choi, W. K., Kwon, T. I., Yeo, Y. K., Lee, H., Song, H. K. and Na, B. K., "Optimal Operation of the Pressure Swing Adsorption (PSA) Process for CO_2 Recovery," *Korean J. Chem. Eng.*, **20**, 617 (2003).

Do, D. D., "Adsorption Analysis," Imperial College Press, London (1988).

Do, D. D. and Wang, K., "Dual Diffusion and Finite Mass Exchange Model for Adsorption Kinetics in Activated Carbon," *AIChE J*., **44**, 68 (1998).

Gupta, R. and Farooq, S., "Numerical Simulation of a Kinetically Controlled Bulk PSA Separation Process Based on a Bidisperse Pore Diffusion Model," In Proceedings of the 8th APCChE Congress, **3**, 1753 (1999).

Kaneko, K., "Molecular Assembly Formation in a Solid Nanospace," *Colloid Surface A*, **109**, 319 (1996).

Kapoor, A. and Yang, R. T., "Kinetic Separation of Methane-Carbon Dioxide Mixture by Adsorption on Molecular Sieve Carbon," *Chem. Eng. Sci.*, **44**, 1723 (1989).

Kim, B. H., Kum, G. H. and Seo, Y. G., "Adsorption of Methane and Ethane into Single-Walled Carbon Nanotubes and Slit-Shaped Carbonaceous Pores," *Korean J. Chem. Eng.*, **20**, 104 (2003).

Micke, A., Bülow, M. and Koricik, M., "A Nonequilibrium Surface Barrier for Sorption Kinetics of p-Ethyltoluene on ZSM-5 Molecular Sieves," *J. Phys. Chem.*, **98**, 924 (1994).

O'koye, I. P., Benham, M. and Thomas, K. M., "Adsorption of Gases and Vapors on Carbon Molecular Sieves," *Langmuir*, **13**, 4054 (1997).

Panczyk, T. and Rudzinski, W., "Kinetics of Gas Adsorption on Strongly Heterogeneous Solid Surfaces: A Statistical Rate Theory Approach," *Korean J. Chem. Eng.*, **21**, 206 (2004).

Park, I. S., "Numerical Analysis of Fixed Bed Adsorption Kinetics Using Orthogonal Collocation," *Korean J. Chem. Eng.*, **19**, 1001 (2002).

Reid, C. R. and Thomas, K. M., "Adsorption of Gases on a Carbon Molecular Sieve Used for Air Separation: linear Adsorptives as Probes for Kinetic Selectivity," *Langmuir*, **15**, 3206 (1999).

Reid, C. R., O'koye, I. P. and Thomas, K. M., "Adsorption of Gases on Carbon Molecular Sieves Used for Air Separation: Spherical Adsorptives as Probes for Kinetic Selectivity," *Langmuir*, **14**, 2415 (1998).

Ross, S. and Oliver, J. P., "On Physical Adsorption," Interscience, New York (1964).

Rutherford, S. W. and Do, D. D., "Characterization of Carbon Molecular Sieve 3A," *Langmuir*, **16**, 7245 (2000).

Ruthven, D. M., Ragahavan, N. S. and Hassan, M. M., "Adsorption and Diffusion of Nitrogen and Oxygen in a Carbon Molecular Sieve," *Chem. Eng. Sci*., **41**, 1325 (1986).

Ruthven, D. M., "Diffusion of Oxygen and Nitrogen in Carbon Molecular Sieve," *Chem. Eng. Sci*., **47**, 4305 (1992).

Rynders, R. M., Rao, M. B. and Sircar, S., "Isotope Exchange Technique for Measurement of Gas Adsorption Equilibria and Kinetics," *AIChE J*., **43**, 2456 (1997).

Smith, J. M., Van Ness, H. C. and Abbott, M. M., "Introduction to Chemical Engineering Thermodynamics," McGraw-Hill, Singapore (1997).

Srinivasan, R., Auvil, S. R. and Schork, J. M., "Mass Transfer in Carbon Molecular Sieves- an Interpretation of Langmuir Kinetics," *The Chemical Engineering Journal*, **57**, 137 (1995).

Suzuki, M., "Adsorption Engineering," Elsevier, Japan (1990).

Talu, O. and Kabel, R. L., "Isosteric Heat of Adsorption and the Vacancy Solution Model," *AIChE J*., **33**, 510 (1987).

Yang, J. Y. and Lee, C. H., "Adsorption Dynamics of a Layered Bed PSA for H_2 Recovery from Coke Oven Gas," *AIChE J*., **44**, 1325 (1998).

Yang, J., Park, M.-W., Chang, J.-W., Ko, S.-M. and Lee, C.-H., "Effects of Pressure Drop in a PSA Process," *Korean J. Chem. Eng.*, **15**, 211 (1998).

Yang, R. T., "Gas Separation by Adsorption Process," Butterworths, Boston (1987).

Yuxun, Y. and Farooq, S., "Sorption and Diffusion of Oxygen and Nitrogen in a Carbon Molecular Sieve," FOA6, Elsevier, 1243 (1998).